Malaysian Journal of Chemistry, 2022, Vol. 24(2), 228-239
(Special Issue: International Conference on Synthesis Chemistry-ICOSC2022, Universiti Teknologi MARA)

Acid Photo Etching Effect of Epoxidized Natural Rubber (ENR) and Polyvinyl Chloride (PVC) as Polymer Binder

Muhammad Afiq Rosli[1], Siti Raihan Hamzah[1], Nur Aien Muhamad[1], Nureel Imanina Abdul Ghani[1], Nadiah Sabihah Md Natar[1], Syahirul Ikhwan Ab Aziz[1], Nur Syazana Nazeri[1], Muhammad Saifulddin Mohd Azami[1], Mohd Azlan Ishak[1], Muhammad Zahiruddin Ramli[2] and Wan Izhan Nawawi[1*]

[1]Faculty of Applied Sciences, Universiti Teknologi MARA, 02600 Arau, Perlis, Malaysia
[2]College of Engineering, Universiti Teknologi MARA Cawangan Pulau Pinang, Kampus Permatang Pauh, 13500 Permatang Pauh, Pulau Pinang
*Corresponding author (e-mail: wi_nawawi@uitm.edu.my)

Epoxidized natural rubber (ENR) and polyvinyl chloride (PVC) were used as polymer binders in immobilizing TiO_2 on glass substrate by using the dip-coating technique. Acid photo etching process was applied to the immobilized TiO_2/ENR/PVC (TEP) samples to determine the reaction and surface transformation with the presence of hydrochloric acid (HCl). The photocatalytic activity of the prepared immobilized TiO_2/ENR/PVC samples was examined on the degradation of reactive red 4 (RR4) dye under a 65 W compact fluorescent lamp. All immobilized TiO_2/ENR/PVC samples under the acid photo etching process (TEP A) expressed higher photoactivity in comparison with to photo etching process (TEP P). TEP A50 (acid photo etching for 50 h) sample has shown the highest photocatalytic degradation where the pseudo 1st order rate constant (k) value was ca. 0.0694 min^{-1}. However, it is not considered as an optimum sample due to the peel-off effect. Therefore, the optimum sample for the acid photo etching process was TEP A40 (acid photo etching for 40 h) with 0.0553 min^{-1}. TEP A40 is 2 times faster as compared with the photoetched immobilized TiO_2/ENR/PVC (TEP P), which is primarily due to the surface transformation and formation of C-OH bond from crosslinking reaction of the polymer binder with the HCl as verified from the FESEM and FTIR analysis.

Key words: Immobilized TiO_2; acid photo etching; polymer binder; crosslinking reaction; photocatalytic degradation

Received: March 2022 ; Accepted: April 2022

Photocatalysis is one of the potential treatment processes to degrade organic products [1]. This process also can be used in air and water purification systems, sterilization, and hydrogen evolution energy fields, including photoelectric conversion [2]. The well-known semiconductor photocatalyst is titanium dioxide (TiO_2) due to its properties being chemically and biologically stable, non-toxic, as well as low in cost [3]. However, the wide bandgap energy (E_g) and high electron-hole recombination have limited the effectiveness of the TiO_2 [4]. Usually, a suspension mode is a normal practice of TiO_2 in degrading organic pollutants due to the high contact of surface area to reactant ratio and light scattering effect [5-6]. However, this practice has difficulty as it requires a post-filtration treatment to separate the nanoparticle TiO_2. This problem can be overcome by developing immobilized TiO_2 where the system makes the TiO_2 to be attached to the support material, thus allowing it to be recycled and continuously used.

There are several approaches to immobilize the TiO_2 onto a solid substrate such as via doctor blade [7], spin coating [8], dip coating [9], and double sided adhesive tape (DSAT) [10]. In addition, some researchers implement polymer as a binder in immobilizing TiO_2, such as polypropylene (PP) granules [11], cellulose fibers [12], polypropylene fibre (PPF) [13], polyvinyl chloride (PVC) [14], polycarbonate (PC), poly(methyl methacrylate) (PMMA) [15], polyvinyl acetate (PVAc) [16], polyethylene sheets [17], thin polyethylene films [18], polystyrene (PS) beads [19], expanded polystyrene (EPS) beads [20], polyethylene glycol [21], fluoro-polymer resins [22], polyethylene terephthalate (PET) bottles [23], poly(styrene)-co-poly(4-vinylpyridine) (PSP4VP) [24], rubber latex (an elastic hydrocarbon polymer) [25], epoxidized natural rubber (ENR) [27], parylene, and tedlar [26]. The addition of polymer can improve the adhesiveness, temperature resisting ability, durability, and absorbance affinity towards pollutants [27]. ENR and PVC are commonly utilized in immobilizing TiO_2 by dip coating method due to their properties in adhesiveness and durability.

†Paper presented at the International Conference on Synthesis Chemistry-ICOSC2022, Universiti Teknologi MARA

Nevertheless, the high content of polymer can decrease the photocatalytic activity due to the less surface contact of TiO_2 and surfactant. Photo etching treatment is introduced to remove the organic and inorganic compounds on the surface of the photo-catalyst. Many researchers have studied the effect of the photo etching treatment on the surface of the immobilized TiO_2/ENR/PVC [29-30]. The ENR-50 additive is removed systematically through a 5h photo etching treatment of the immobilized TiO_2 system [29]. It is also stated that there is a crosslinking reaction between the ENR and PVC, which supports the immobilized TiO_2 onto the glass substrate. Nawi et al. [30] stated that the PVC also may turn into polyene during the photo etching treatment, thus enhancing the photocatalytic activity. However, no research has been reported regarding the acid photo etching treatment on the surface of immobilized TiO_2. Hence, this study aims to immobilize TiO_2 with ENR and PVC as polymer binder along with the determination of the acid photo etching treatment effect for photocatalysis enhancement of RR4 dye under a 65 W compact fluorescent lamp.

EXPERIMENTAL

1. Chemicals

The chemical used was titanium(IV) oxide (TiO_2), Degussa P25, 80:20 ratio of anatase and rutile, epoxidized natural rubber (50% epoxidation) (ENR50) from Guthrie Group Limited. Poly (vinyl) chloride (PVC) powder from petrochemicals (Malaysia) Sdn. Bhd. Acetone was obtained from QRec, and dichloromethane was purchased from R&M Chemicals. For the dye, reactive red 4 (RR4) dye as a model pollutant was purchased from Sigma Aldrich.

2. Preparation of Epoxidized Natural Rubber (ENR50) Solution

Epoxidized natural rubber (ENR50) solutions was prepared by refluxing 24. 8 ± 0.05 g of ENR50 in 250 mL of toluene at 88 ± 2 °C for 192 h until a sticky solution was formed. The prepared ENR solution was transferred into a screw cap 250 mL Schott bottle for the preparation of TiO_2 formulation.

3. Preparation of Polyvinyl Chloride (PVC) Solution

Polyvinyl chloride (PVC) solution was prepared by using 4.0 g of PVC powder dissolved in 175 mL dichloromethane under stirring process for about 60 minutes. A homogenized PVC solution was then placed into a screw cap 250 mL Schott bottle for the preparation of TiO_2 formulation.

4. Preparation of TiO_2/ENR/PVC Formulation

About 20.0 g ENR and 4.0 g PVC solutions were then mixed by using a magnetic stirrer for 2 hours. After the mixed solution homogenized well, 30.0 g of TiO_2 was added slowly into the mixture under continuous stirring process for 36 hours.

5. Preparation of Immobilized TiO_2/ENR/PVC

A clean glass plate was used as support material to prepare an immobilized TiO_2/ENR/PVC via a dip-coating technique. The weight of the glass plate was been obtained by using an analytical balance. The dip-coating technique was carried out by pouring TiO_2 formulation into a coating cell made from glass. After that, a clean glass plate was dipped for 5 seconds into the dip-coating solution, covering up to 5.6 cm depth (26.3 cm^2), and later pulled up manually with a consistent pulling rate. Afterward, the coated glass plate was dried using a hot air blower and the smoothed side of the coated glass scrapped off prior the final weight was recorded.

6. Photo etching and Acid Photo Etching in Immobilized TiO_2 with ENR and PVC

In the photo etching procedure, 20 mL of distilled water was transferred into the glass cell. The Immobilized TiO_2/ENR/PVC was immersed and the light was irradiated using a UVA lamp under aerated conditions. The coated glass plate was undergo photo etching for 1, 5, 10, 30, 40, and 50 h. The procedure for acid photo etching was the same as the photo etching process by replacing the distilled water with 1. 0 N of 20 mL hydrochloric acid (HCl) for 1, 5, 10, 30, 40, and 50 h. After being immersed in the acid as stated earlier, the glass plate was pulled away from the glass cell and rinsed with distilled water. The rinsed glass plate was undergo washing process for one hour prior photocatalysis degradation process.

7. Characterization of TiO_2/ENR/PVC

The absorbance from photocatalytic degradation of RR4 was analyzed using UV – Visible spectroscopy at 517 nm wavelength. Unmodified and modified TiO_2/ENR/PVC were characterized by Fourier Transform Infrared – Attenuated Total reflectance (FTIR – ATR) analyzer (Perkin-Elmer, model system 2000 FTIR) to see the changes of the functional groups of the samples. Scanning Electron Microscope (SEM) analyzer model LEO SUPRA 50 VP Field Emission SEM and 3D Optical Profilometer (PEMTRON HAWK 3D WT-250) were used to analyze the surface morphology of the samples. X-ray diffraction (XRD) analysis used Bruker D8 Advance diffractometer was conducted to see the

crystallinity of the samples.

8. Photocatalytic Degradation

Photocatalytic activity degradation performances was analyzed by using UV-Visible spectroscopy at 517 nm wavelength due to the max absorbance of the RR4 dye. Anionic azo dye which is RR4 dye was used as the model pollutant due to its application in the most textile industries. For the degradation performances of the photocatalyst, 10 mL of 30 ppm RR4 dye solution was poured in the fabricated glass cell with aeration flow rate, 10 mL/min and 55W light irradiation. 3 mL of the treated dye were collected at every 15 min interval and the absorbances were determined by using UV-Vis spectroscopy at 517 nm wavelength. The graph were plotted for the determination of the k value and the linear correlation value. The results were converted into ln C0/C where C0 the absorbance of the initial concentration and C is the absorbance at any time (t), thus the values were plotted against irradiation or contact time. Based on the Langmuir-Hinshelwood rate model, the slope of the linear line was taken as the pseudo first order rate constant.

RESULTS AND DISCUSSION

1. Characterization

The surface morphologies of the TEP P and TEP A40 samples via Field Emission Scanning Electron Microscopy (FESEM) under 5000x magnification are shown in Figure 1. The surface of the photoetched (TEP P) sample depicts some clusters of nanoparticles that form bigger spheres and have a sponge-like layer structure on the surface. This sample also reveals the formation of tiny porosity particles.

However, the surface of immobilized TiO_2/ ENR/PVC was modified by immersing it in the acid with the presence of UV light. The acid photo etching treatment has affected the formation of active sites on the TiO_2 surface. A melted-like layer appears on the surface of TEP A40 when HCl is applied to the immobilized TiO_2/ENR/PVC. According to Sriwong et al. [31], TiO_2 decreases due to the high amount of natural rubber. The presence of ENR may cover the surface-active sites of TiO_2.

The surface of TEP P and TEP A40 were characterized by a 3D optical profilometer to visualize the surface porosity and roughness. Based on the 2D surface profile in Figure 2 (a-b), the porosity of the samples can be determined by the height of the surface revealed in the colour indicator. The deepest height is shown in red colour while the tallest height is in blue. Figure 2 (c-d) shows the 3D surface profile, which illustrates that the surface of TEP A40 was more porous compared to TEP P.

The parameters in the 2D-surface roughness category are average roughness (R_a) and familiar root mean square roughness (R_q). Both of these parameters were given by the following equations (Eq. 1-2) [32]:

$$R_a = (1/N) \sum_{J=1}^{N} |Z_J| \qquad \text{Equation 1}$$

Where N is the total number of measured points, and Z_J is the vertical height deviation from the average height of the surface.

$$R_q = \sqrt{(\sum (Z_J)^2) / N} \qquad \text{Equation 2}$$

In this equation, Z_J is the vertical deviation with respect to a mean line for the *jth* point of the total N measured points.

R_a values for TEP P and TEP A40 were 3877.32 nm and 6473.59 nm, while the R_q values were 4873.04 nm and 8011.85 nm, respectively. The larger surface structures of TiO_2/ENR/PVC with high roughness and high porous surfaces allow more photocatalytic reactions than surfaces with low morphological structures that can lower the photo-catalytic activity as well as RR4 degradation [33].

The surface roughness of TEP A40 is higher than TEP P due to the high porosity as ENR-50 leach out from the immobilized TiO_2 which is supported by the previous XRD and FTIR analysis.

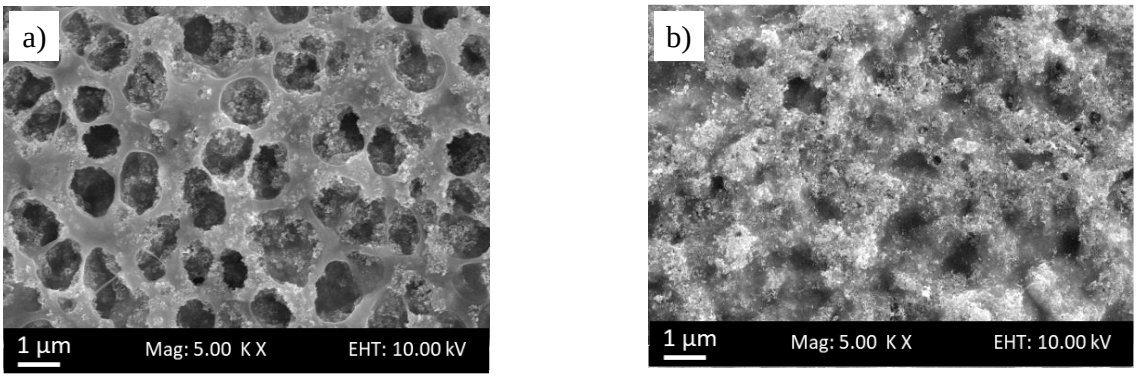

Figure 1. Field Emission Scanning Electron Microscopy (FESEM) results of a) TEP P and b) TEP A40 sample under 5000x magnification.

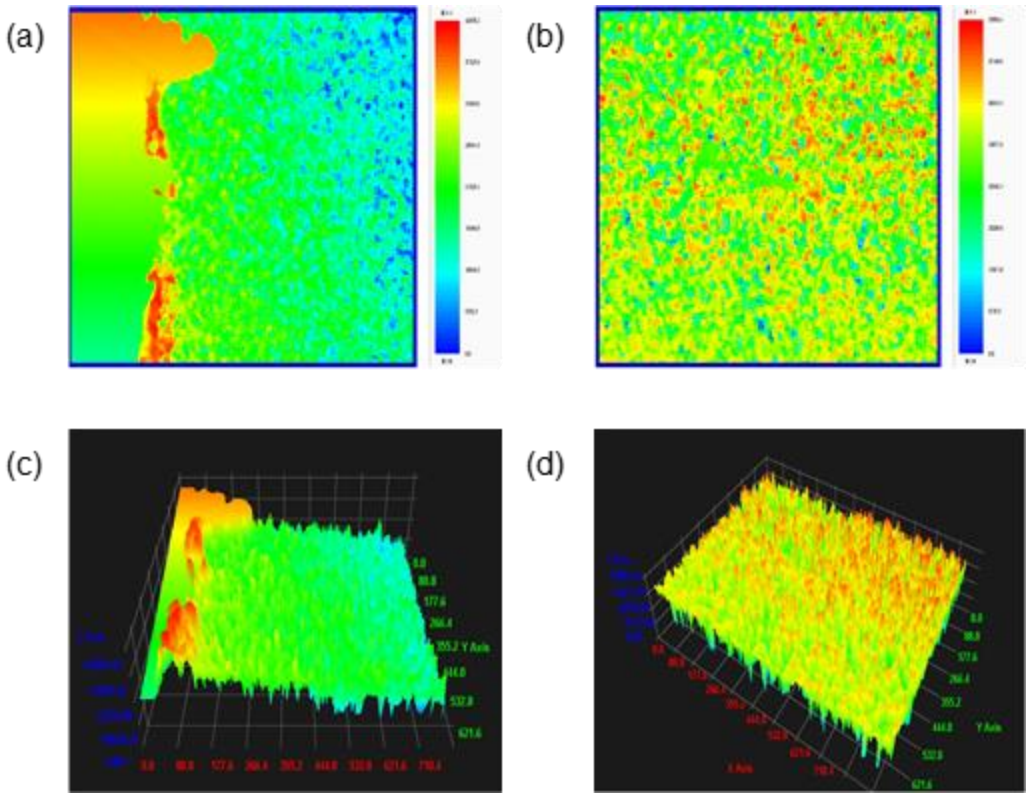

Figure 2. a) 2D surface profile and b) 3D surface profile of TEP P and c) 2D surface profile and d) 3D surface profile of TEP A40, respectively

Figure 3 shows XRD patterns for unmodified (TEP 0), photoetched (TEP P), and optimal acid photoetched (TEP A40) TiO_2/ENR/PVC in the anatase phase. According to the JCPDS databases, the standard spectrum for XRD, the figure shows a clear reflection at two values of 26.054° and 48.766°, which indicate strong diffraction of TiO_2 anatase. Due to the absence of ENR, the strong diffraction and intensity of TiO_2 increased from TEP 0 to TEP A40 at a value of 26.054°, resulting in the formation of TiO_2 crystals.

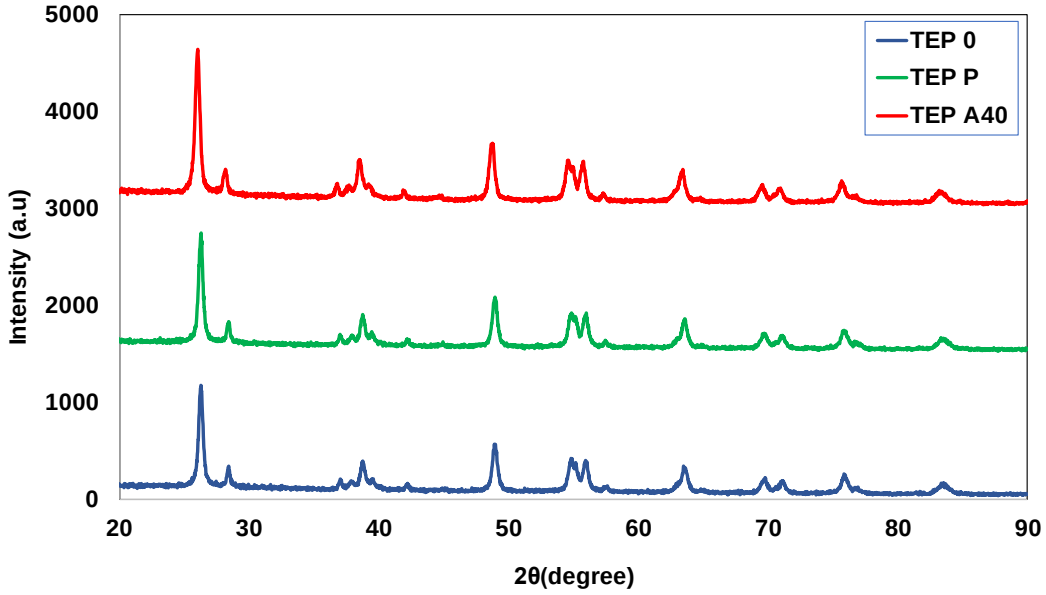

Figure 3. XRD patterns of a) unmodified TiO_2/ENR/PVC (TEP 0), b) photoetched TiO_2/ENR/PVC (TEP P), and c) 40 h acid photoetched TiO_2/ENR/PVC (TEP A40)**.**

Table 1. Crystallinity Index (CI) % for TEP 0, TEP P, and TEP A40

Sample	TEP 0	TEP P	TEP A40
Crystallinity Index (%)	37.68	42.398	42.91

The intensity of the XRD peaked at 48.766° showed broad diffraction peaks, indicating a relatively tiny size of TiO_2 crystallite [34]. Furthermore, it was obvious from the crystallinity index, which was derived by dividing the area of crystalline peaks for TiO_2 anatase by the total number of peaks, i.e., amorphous and crystalline, as shown in Eq. 3. Table 1 shows the crystallinity index for TEP 0, TEP P, and TEP A40. Based on the results obtained, TEP A40 has the highest crystallinity index, which is 42.91 %.

Crystallinity index (CI) = Area CP / Area CAP Equation 3

Where:
Area CP = Area of all the crystalline peaks
Area CAP = Area of all the crystalline and amorphous peaks.

Figure 4 represents the FTIR spectra from 600 to 1100 cm^{-1} for six different types of immobilized TiO_2/ENR/PVC samples. The intensity peak of the acid photoetching treatment that appeared at 664 cm^{-1} of the shown some increment compared to the unmodified TiO_2/ENR/PVC, photo-etched TiO_2/ENR/PVC, and acid photo-etched TiO_2/ENR/PVC. The peak has been identified as a Ti – O stretching band, which is a TiO_2 characteristic peak. The addition of acid reduces the ENR bound to TiO_2 and increases the intensity of the Ti – O peak [35]. The expectation of this study is TiO_2 binds with ENR/PVC to allow the ring opening to occur against the epoxide in the ENR and a crosslinking process will take place between the C – O bond (aliphatic ether) of the ENR and the PVC compound. The ring-opening for the ENR molecules and crosslinking for ENR/PVC were seen and needed to be confirmed via FTIR. The FTIR spectrum of unmodified TiO_2/ENR/PVC, photo-etched TiO_2/ENR/PVC, and acid photo-etched TiO_2/ENR50/PVC are shown in Figure 4 respectively.

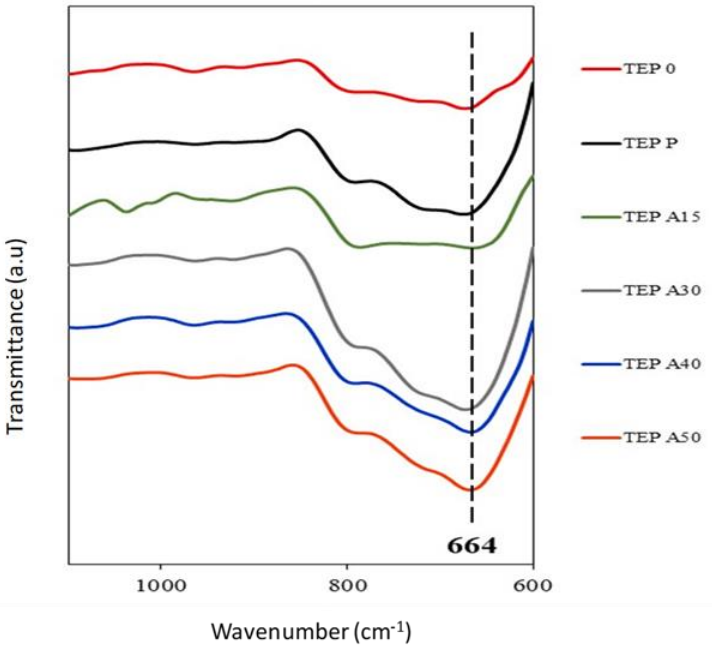

Figure 4. FTIR spectrum at the band 600 – 1100 cm^{-1}

Figure 5 shows a comparison of TEP 0, TEP P, and TEP A40 in terms of ring-opening and crosslinking process between two polymers. The formation of ring-opening from the C – O bond on ENR molecules happened as predicted at the bands 1090 cm^{-1}. The intensity increased from TEP 0 to TEP A40 in the 1196 cm^{-1} band, with smaller peaks apparent. According to the FTIR spectrum table, it is peak C – O for tertiary alcohol. A functional group corresponding to C – Cl stretching peak could be seen in the 804 cm^{-1} bands. The peak at 1352 cm^{-1} and 1427 cm^{-1} bands indicate a C – H bending from aliphatic bonding caused by the destruction of C – H_3 bonds from ENR molecules. While the absorption bands 1655 cm^{-1} and 2175 cm^{-1} reveal the peak of C = C from ENR, 2930 cm-1 shows the peak of C – H_2 asymmetrical stretching for an aliphatic group. A large peak appears in the absorption band of 3282 cm^{-1}, where it is associated with O – H. The FTIR spectrum shows that only ring opening on the ENR structure occurs and crosslinking between ENR and PVC does not occur under acid-etched in the presence of UV light.

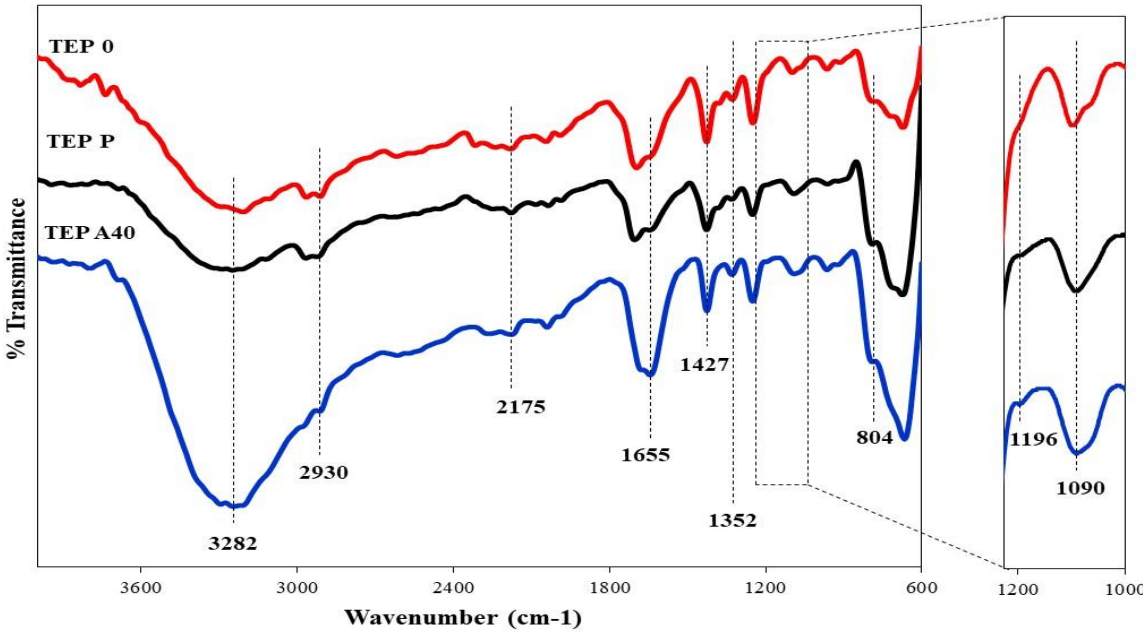

Figure 5. FTIR spectra at the band 600 – 4000 cm^{-1}

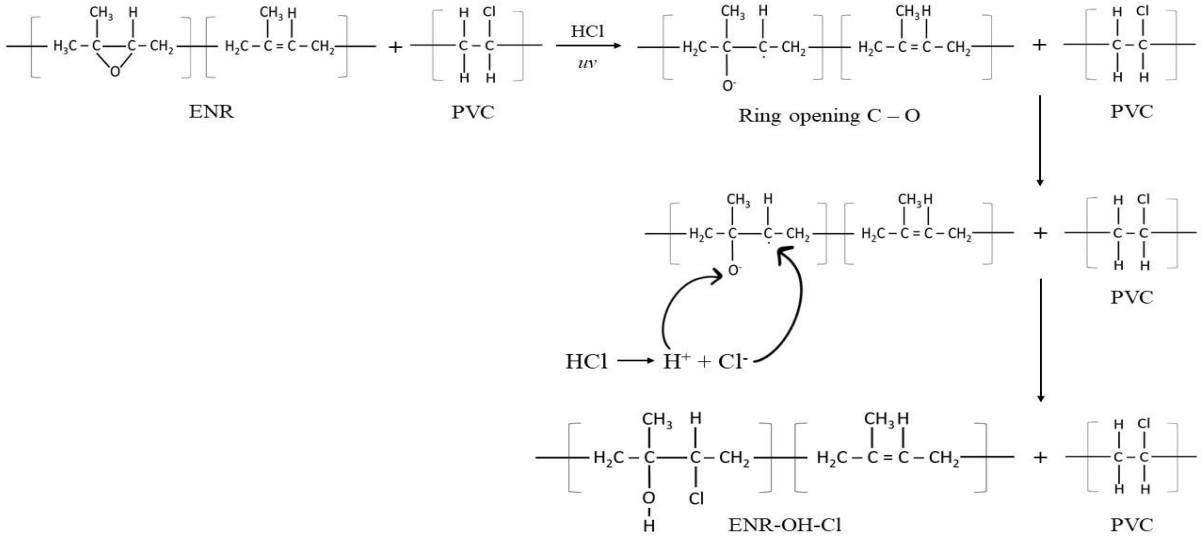

Figure 6. Proposed mechanism of ring opening for ENR

The proposed mechanism of the ENR and PVC in the presence of acid is depicted in Figure 6. The ring opening mechanism occurs to the ENR structure from the structure. It is expected that in the presence of acid and UV radiation, the production of C – OH occurs. However, it is assumed that the crosslinking does not occur between ENR and PVC structures; hence the formation of ring openings has increased photo-catalytic activity as verified by several other characterizations.

Photoluminescence (PL) spectroscopy has been widely used to explore the efficiency of charge trapping, immigration, and transfer and to acknowledge the recombination of electron hole pairs in the semiconductor particles [28]. PL analysis was done for TEP P and TEP A40 samples which the spectra are plotted as shown in Figure 7. PL signals result for TiO_2 semiconductors is usually from the recombination of photo-induced charge carriers. Based on Figure 7, the maxima peak for TEP P was at 452 nm due to the band-band recombination process of the induced charge carriers, while TEP A40 reached the maxima peak at 588 nm due to the excitonic PL signal primarily from the surface oxygen vacancies and defects of semiconductors. TEP A40 has a low recombination rate of electron-hole pairs, thus higher photo-catalytic activity can be achieved since it has low PL intensity of the band-band peak.

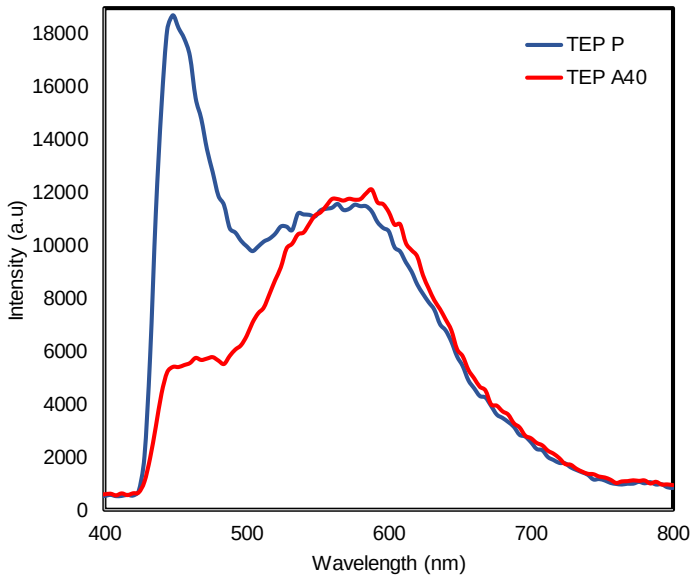

Figure 7. Photoluminescence (PL) spectra of TEP P and TEP A40.

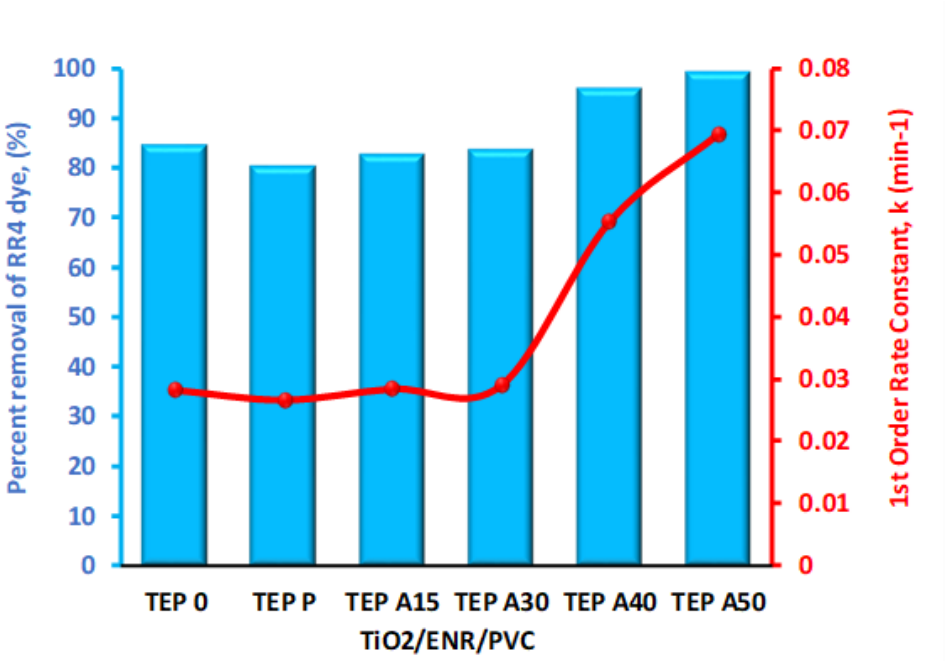

Figure 8. Pseudo first-order rate is constant for photocatalytic degradation of RR4 for the immobilized TiO_2/ENR/PVC.

2. Photodegradation of Immobilized TiO_2/ ENR/PVC

Photocatalytic degradation activity of RR4 dye was determined by the absorbance of the RR4 towards the immobilized TiO_2/ENR/PVC plate. The comparison was made by observing the differences of rate constant between three conditions which are unmodified immobilized TiO_2/ENR/PVC (TEP 0), photoetched immobilized TiO_2/ENR/PVC (TEP P), and acid photoetched immobilized TiO_2/ENR/PVC (TEP A15, TEP A30, TEP A40, TEP A50) that have been irradiated under UV light. Figure 6 shows the percent degradation and rate constant (k) value for each sample. The increment of percent degradation and k value is perpendicular to the time of the acid photo etching. Even though TEP A50 has the highest value of k compared to other samples, the optimum sample is TEP A40 with a 0.0553 min^{-1} k value. TEP A50 was not considered optimal due to the TiO_2/ENR/PVC composite peeling off from the glass substrate by itself when the acid photo etching time was prolonged. The high molarity of HCl with the presence of UV light for a long period can dissolve the TiO_2/ENR/PVC composite layer on the plate.

Figure 8 is supported by Figure 9 and Figure 10, which show the percent remaining of RR4 dye and linear correlation coefficient, R^2 value for each sample, respectively. In Figure 9, the percent remaining at 1 hour decreases with the increment of acid photo etching time. The lowest percent remaining is TEP A50, followed by TEP A40. Based on Figure 10, the order of the reaction was found in the range 0.9-1.0. Hence, this reaction has successfully followed the Pseudo first-order reaction and confirmed that no absorption process happened.

Figure 11 depicts the component on the surface of the immobilized TiO_2 before and after the acid photo etching treatment. A ring-opening reaction occurred in the presence of UV light on the ENR structure which resulted in the formation of a C – O bond. However, the crosslink reaction recombination of electron hole pairs. The ENR-OH-Cl will scavenge the electron produced from the conduction band in TiO_2 and prevent them from recombining with the hole located at the valence band. At this state, a better photocatalytic activity can be achieved as the tendency of superoxide ions formation is higher.

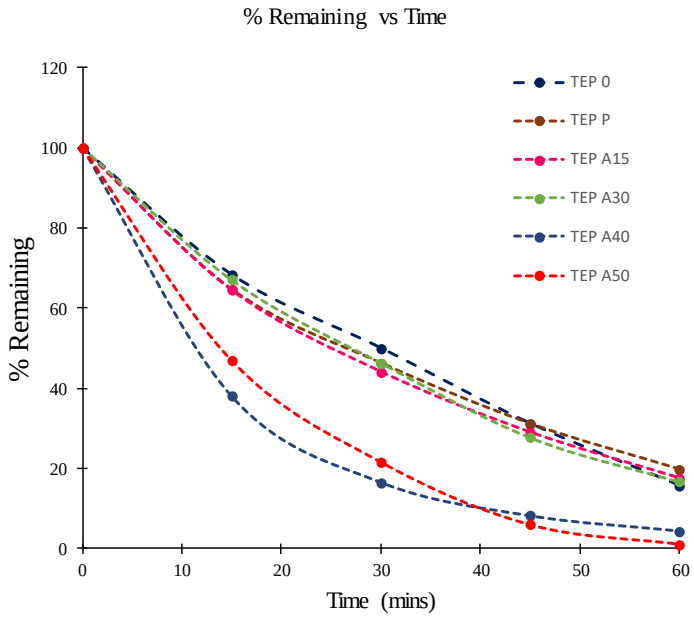

Figure 9. Percent remaining of RR4 dye for each sample during photocatalytic degradation for 1 hour.

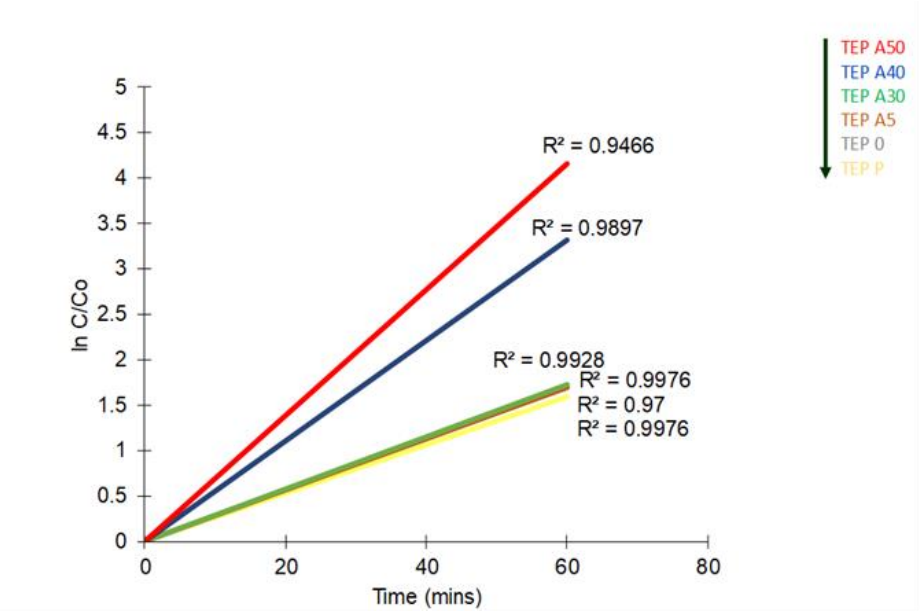

Figure 10. Linear correlation coefficient, R_2 for each sample

between ENR and PVC does not occur in the presence of HCl and the ENR structure may react with the ion from acid, which is H^+ and $Cl,^-$ thus forming the C – OH bond. Based on the PL intensity result shown in Figure 7, the ENR-OH-Cl substances may act as electron scavengers as there is low

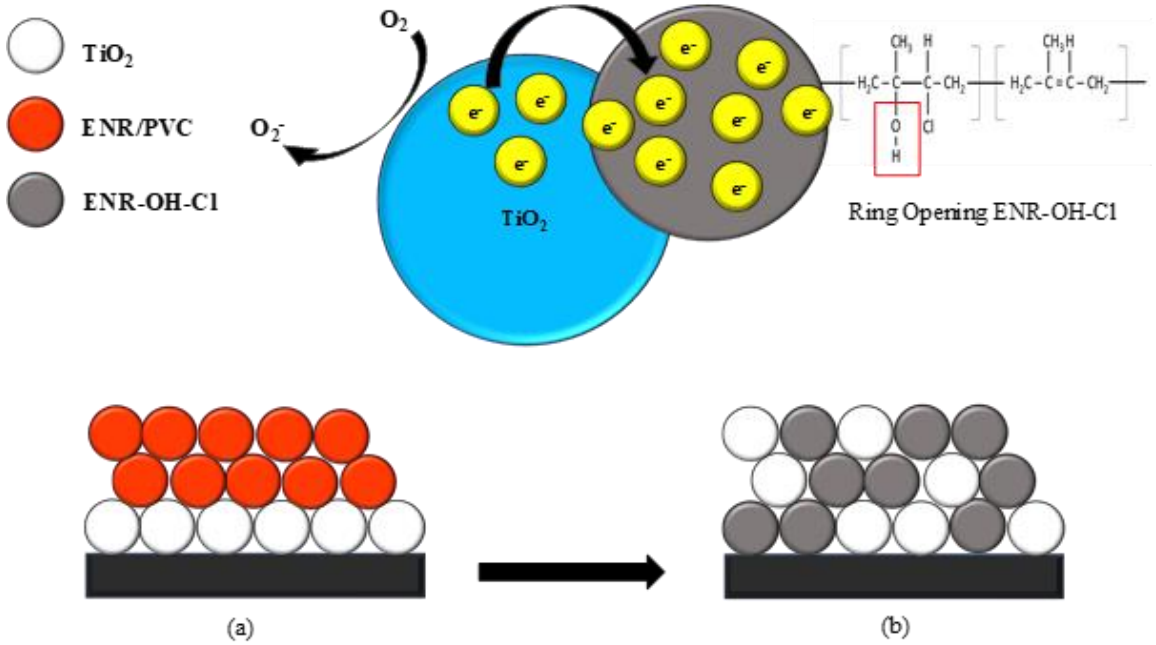

Figure 11. Schematic diagram of electron injection and immobilized TiO_2 surface before and after acid photo etching treatment.

CONCLUSION

This work discovered the effect of acid photo etching on immobilized TiO_2/ENR/PVC and the reaction between the polymer binder and hydrochloric acid during the acid photo etching treatment. The enhancement of photocatalytic activity has been achieved by implementing the acid photo etching treatment onto the immobilized TiO_2/ENR/PVC before the photocatalytic degradation of RR4 dye. This statement has been explained by the characterization of FESEM, 3D profile, and XRD pattern. In addition, the FTIR spectra show the high intensity of the OH bond, which indicates the increment of the OH bond produced. Hence, the mechanism reaction through the acid photo etching treatment can be proposed by the FTIR analysis. This significant discovery can be one of the approaches to enhance the photocatalytic activity of other immobilized catalysts.

ACKNOWLEDGMENT

The authors would like to thank Universiti Teknologi MARA (UiTM) for providing financial support under the internal grant “Dana Pembudayaan Penyelidikan Dalaman (DPPD)” code no: 600-TNCPI 5/3/DDN (09) (010/2022) in conducting this study. We would also like to acknowledge Universiti Malaysia Perlis (UniMAP) and Universiti Teknologi MARA (UiTM) for providing all the facilities.

REFERENCES

1. Dong, H., Zeng, G., Tang, L., Fan, C., Zhang, C., He, X. & He, Y. (2015) An overview on limitations of TiO_2-based particles for photocatalytic degradation of organic pollutants and the corresponding countermeasures. *Water research*, **79**, 128–146.

2. Zhang, Y., Hu, H., Kang, W., Qiu, G., Liang, R., Deng, L. & Yuan, H. (2020) Enhancing hydrogen evolution by photoelectrocatalysis of water splitting over a CdS flowers-loaded TiO_2 nanotube array film on the Ti foil substrate. *Ceramics International*, **46(11)**, 17606–17613.

3. Iqbal, A., Ibrahim, N. H., Rahman, N. R. A., Saharudin, K. A., Adam, F., Sreekantan, S. & Wilson, L. D. (2020) ZnO Surface Doping to Enhance the Photocatalytic Activity of Lithium Titanate/TiO_2 for Methylene Blue Photo-degradation under Visible Light Irradiation. *Surfaces*, **3(3)**, 301–318.

4. Bahrudin N. N., Nawi M. A., Nawawi W. I. (2021) Enhanced photocatalytic decolorization of methyl orange dye and its mineralization pathway by immobilized TiO_2/polyaniline. *Research on Chemical Intermediates*, **45**, 2771–2795.

5. Li, Q., Chen, X., Zhuang, J. & Chen, X. (2016) Decontaminating soil organic pollutants with manufactured nanoparticles. *Environmental Science and Pollution Research*, **23(12)**, 11533–11548.

6. Zahid, M., Nadeem, N., Hanif, M. A., Bhatti, I.

A., Bhatti, H. N. & Mustafa, G. (2019) Metal ferrites and their graphene-based nano-composites: synthesis, characterization, and applications in wastewater treatment. In *Magnetic nanostructures, Springer, Cham.*, 181–212.

7. Utami, F. D., Rahman, D. Y., Sustini, E. & Abdullah, M. (2019) Immobilization of TiO_2 on transparent plastic and its application in photo-catalytic wastewater treatment. In *Journal of Physics: Conference Series, IOP Publishing*, **1171(1)**, 012030.

8. Prawira, R. A. & Ariyanti, D. (2021) Recent study on TiO_2 based Self-Cleaning Coating. In *IOP Conference Series: Materials Science and Engineering, IOP Publishing*, **1053(1)**, 012061.

9. El-Mekkawi, D. M., Nady, N., Abdelwahab, N. A., Mohamed, W. A. & Abdel-Mottaleb, M. S. A. (2016) Flexible bench-scale recirculating flow CPC photoreactor for solar photocatalytic degradation of methylene blue using removable TiO_2 immobilized on PET sheets. *International Journal of Photoenergy*.

10. Ismail, W. I. N. W., Ain, S. K., Zaharudin, R., Jawad, A. H., Ishak, M. A. M., Ismail, K., Sahid, S. (2015) New TiO_2/DSAT Immobilization System for Photodegradation of Anionic and Cationic Dyes. *International Journal of Photoenergy*, 1-7.

11. Rokhmat, M., Wibowo, E. & Abdullah, M. (2017) Coating TiO_2 nanoparticles on the surface of transparent plastic granules using combined electrostatic and heating methods for the photo-catalytic degradation of organic pollutants in water. *Environmental nanotechnology, monitoring & management*, **8**, 1–10.

12. Pan, Y., Liu, B., Hu, H., Jiang, H., Wei, F., Zhou, M. & Huang, J. (2019) Preparation and photo-catalytic performance of the rod-shaped Ni-NiO/TiO_2 hollow composite structure based on metallization cellulose fibers and TBOT. *Vacuum*, **159**, 1–8.

13. Reddy, K. R., Jyothi, M. S., Raghu, A. V., Sadhu, V., Naveen, S. & Aminabhavi, T. M. (2020) Nanocarbons-supported and polymers-supported titanium dioxide nanostructures as efficient photocatalysts for remediation of contaminated wastewater and hydrogen production. In *Nano-photocatalysis and Environmental Applications, Springer, Cham.*, 139–169.

14. Bui, D. P., Huu Pham, H., Minh Cao, T. & Van Pham, V. (2020) Preparation of conjugated polyvinyl chloride/TiO_2 nanotubes for Rhodamine B photocatalytic degradation under visible light. *Journal of Chemical Technology & Biotechnology*, **95(10)**, 2707–2714.

15. Cámara, R. M., Portela, R., Gutierrez-Martin, F. & Sánchez, B. (2016) Photocatalytic activity of TiO_2 films prepared by surfactant-mediated sol–gel methods over commercial polymer substrates. *Chemical Engineering Journal*, **283**, 535–543.

16. Petković, G., Vukoje, M., Bota, J. & Pasanec Preprotić, S. (2019) Enhancement of polyvinyl acetate (PVAc) adhesion performance by SiO_2 and TiO_2 nanoparticles. *Coatings*, **9(11)**, 707.

17. Nawawi, W. I., Zaharudin, R., Zuliahani, A., Shukri, D. S., Azis, T. F. & Razali, Z. (2017) Immobilized TiO_2-polyethylene glycol: effects of aeration and pH of methylene blue dye. *Applied Sciences*, **7(5)**, 508.

18. Xing, Y., Li, X., Zhang, L., Xu, Q., Che, Z., Li, W. & Li, K. (2012) Effect of TiO_2 nanoparticles on the antibacterial and physical properties of polyethylene-based film. *Progress in Organic Coatings*, **73(2-3)**, 219–224.

19. Altın, I. & Sökmen, M. (2014) Preparation of TiO_2-polystyrene photocatalyst from waste material and its usability for removal of various pollutants. *Applied Catalysis B: Environmental*, **144**, 694–701.

20. Varnagiris, S., Urbonavicius, M., Tuckute, S., Lelis, M. & Milcius, D. (2017). Development of photocatalytically active TiO_2 thin films on expanded polystyrene foam using magnetron sputtering. *Vacuum*, **143**, 28–35.

21. Ismail, W. I. N., Zaharudin, R., Zuliahani, A., Shukri, D. S., Azis, T. F., Razali Z. (2017) Immobilized TiO_2-Polyethylene Glycol: Effects of Aeration and pH of Methylene Blue Dye. *Applied Sciences*, **7(5)**, 1–10.

22. Arturi, K. R., Jepsen, H., Callsen, J. N., Søgaard, E. G. & Simonsen, M. E. (2016) Superhydro-philicity and durability of fluoropolymer-TiO_2 coatings. *Progress in Organic Coatings*, **90**, 132–138.

23. Ribeiro, L. N., Fonseca, A. C., da Silva, E. F., Oliveira, E. D., Ribeiro, A. T., Maranhão, L. C. & Almeida, L. C. (2020) Residue-based TiO_2/PET photocatalytic films for the degradation of textile dyes: A step in the development of green monolith reactors. *Chemical Engineering and*

Processing-Process Intensification, **147**, 107792.

24. Reddy, K. R., Jyothi, M. S., Raghu, A. V., Sadhu, V., Naveen, S. & Aminabhavi, T. M. (2020) Nano-carbons-supported and polymers-supported titanium dioxide nanostructures as efficient photocatalysts for remediation of contaminated wastewater and hydrogen production. In *Nano-photocatalysis and Environmental Applications, Springer, Cham*., 139–169.

25. Toh-ae, P., Junhasavasdikul, B., Lopattananon, N. & Sahakaro, K. (2016) Mechanical properties and stability towards heat and UV irradiation of natural rubber/nanotitanium dioxide composites. *Procedia Chemistry*, **19**, 139–147.

26. Singh, S., Mahalingam, H. & Singh, P. K. (2013) Polymer-supported titanium dioxide photo-catalysts for environmental remediation: A review. *Applied Catalysis A: General*, **462**, 178–195.

27. Sabri, N. A., Nawi, M. A. & Bakar, N. A. (2018) Recyclable immobilized carbon coated nitrogen doped TiO_2 for photocatalytic degradation of quinclorac under UV–vis and visible light. *Journal of environmental chemical engineering*, **6(1)**, 898–905.

28. Razak, S., Nawi, M. A. & Haitham, K. (2014) Fabrication, characterization and application of a reusable immobilized TiO_2–PANI photocatalyst plate for the removal of reactive red 4 dye. *Applied surface science*, **319**, 90–98.

29. Nawi, M. A. & Zain, S. M. (2012) Enhancing the surface properties of the immobilized Degussa P-25 TiO_2 for the efficient photocatalytic removal of methylene blue from aqueous solution. *Applied Surface Science*, **258(16)**, 6148–6157.

30. Nawi, M. A., Ngoh, Y. S. & Zain, S. M. (2012) Photoetching of Immobilized TiO_2-ENR50-PVC Composite for Improved Photocatalytic Activity. *International Journal of Photoenergy*.

31. Sriwong, C., Choojun, K. & Sriwong, S. (2019) High photocatalytic performance of 3D porous-structured TiO 2@ natural rubber hybrid sheet on the removal of indigo carmine dye in water. *SN Applied Sciences*, **1(8)**, 1–10.

32. Sadeghi, S. M., Vaezi, M., Kazemzadeh, A. & Jamjah, R. (2021) 3D networks of TiO_2 nanofibers fabricated by sol-gel/electrospinning/ calcination combined method: Valuation of morphology and surface roughness parameters. *Materials Science and Engineering: B*, **271**, 115254.

33. Becerril-Altamirano, N. L., López, R. H., Reyes, L. G., Parra, A. S., López, R. R., Jiménez, A. M. & Hernández-Pérez, I. (2019) Reactive Black-5 Photodegradation by TiO_2 Thin Films Prepared by Ultrasonic Spray. In *Journal of Physics: Conference Series, IOP Publishing*, **1221(1)**, 012027).

34. Ijadpanah-Saravy, H., Safari, M., Khodadadi-Darban, A. & Rezaei, A. (2014) Synthesis of titanium dioxide nanoparticles for photocatalytic degradation of cyanide in wastewater. *Analytical Letters*, **47(10)**, 1772–1782.

35. Zhang, H., Wang, X., Li, N., Xia, J., Meng, Q., Ding, J. & Lu, J. (2018) Synthesis and characterization of TiO 2/graphene oxide nanocomposites for photoreduction of heavy metal ions in reverse osmosis concentrate. *RSC advances*, **8(60)**, 34241–34251.

36. Rahman, Z. & Thomas, L. (2021) Chemical-Assisted Microbially Mediated Chromium (Cr) (VI) Reduction Under the Influence of Various Electron Donors, Redox Mediators, and Other Additives: An Outlook on Enhanced Cr (VI) Removal. *Frontiers in Microbiology*, **11**, 3503.